Jurnal Kejuruteraan 37(3) 2025: 1553-1561
https://doi.org/10.17576/jkukm-2025-37(3)-36

Study on ZL205A Matrix Composites Reinforced with in-situ TiB_2 particles

Jingchuan Tang*, Mohd Zaidi Omar & Intan Fadhlina Mohamed

Department of Mechanical and Manufacturing Engineering,
Faculty of Engineering and Built Environment, Universiti Kebangsaan Malaysia, 43600 Bangi, Selangor, MALAYSIA.

**Corresponding author: p126473@siswa.ukm.edu.my*

Received 30 June 2024, Received in revised form 10 February 2025
Accepted 10 March 2025, Available online 30 May 2025

ABSTRACT

As various faculties and governments issued critical statements to reduce greenhouse gas emissions, effectively reducing carbon emissions from vehicles can have large ecological and economic benefits. The use of aluminium alloys in the design and manufacture of automobiles can effectively reduce the weight of automobiles and thus reduce carbon emissions. Aluminium composites have better mechanical properties than traditional aluminium alloys and can be used in more environments. In this paper, it is found that the addition of TiB_2 particles in the casting process of ZL205A aluminium alloy can effectively refine the grain size, which refined from the traditional ZL205A aluminium alloy of 195um, to 162um (0.1wt.% TiB_2), 148um (0.5wt.% TiB_2), 134um (1wt.% TiB_2), 122um (2wt.% TiB_2), 120um (3wt.% TiB_2). The fabricated ZL205A/ TiB_2 composites have better mechanical properties. Especially when TiB_2 reaches 2wt.%, Ultimate tensile strength (UTS), Yield Strength (YS), Elongation (EL) and wear resistance reach the maximum value. However, when TiB_2 further reaches 3 wt.%, the mechanical properties show a decline compared to the 2 wt.% TiB_2 specimens. This may be due to the occurrence of agglomeration of excess TiB_2. In future studies, more advanced analytical methods and equipment would be used to further analyse the strengthening mechanism of TiB_2 on ZL205A.

Keywords: ZL205A; TiB_2; composite; mechanical properties; in-situ

INTRODUCTION

In recent years, *various faculties and governments issued critical statements to reduce greenhouse gas emissions* (Aldy et al. 2024). Light weighting the design and manufacture of vehicles is a good option for the automotive industry. Light weighting (LW) of vehicles can reduce both oil consumption and greenhouse gas emissions. Aluminum alloys are increasingly used in automotive structures due to their high strength and light weight (Fadzil et al. 2021; Graf 2021). Despite such advantages, aluminium alloys have limited their growth in the automotive industry due to their higher cost, manufacturing challenges, and inferior strength compared to steel. Aluminium Matrix Composites (AMCs) are attracting more and more attention in the automotive sector due to their superior properties compared to common aluminium alloys (Srivyas et al. 2019; Chandel et al. 2021).

AMCs are usually made by combining different particles as strengthening materials with an aluminum alloy matrix. AMCs have the outstanding strength and plasticity from metals and the excellent stiffness and high modulus obtained from the reinforcements. (Kumar et al. 2024). Nowadays, AMCs are rapidly being used in different areas of the automotive industry. These materials are immiscible with each other and have universally desired properties. For example, particles or filaments such as SiC, Al_2O_3, TiB_2, and carbon are essentially used as reinforcement materials for AMCs (Srivyas et al. 2019). TiB_2 particles are characterized by the low density of 4.5g/cm3, a high modulus of elasticity of 565GPa and excellent wear resistance. It has received attention from scholars in the last few years. (Bhowmik et al. 2021; Dayanand et al. 2020). Currently, there are two main methods for the preparation of aluminium-based TiB_2 composites, one is the ex-situ addition and the other is the in-situ synthesis. In the external addition method, TiB_2 particles are synthesized and refined

externally and then added to the melt for fabrication. The in-situ method involves adding the salt needed to synthesize TiB_2 to the melt, where it reacts to each other and produces TiB_2 particles. According to the study of other scholars, the in-situ TiB_2 particles exhibit better clean interface and strong interfacial adhesion (Dong et al. 2021; Malaki et al. 2019). Xie et al. find the properties of 2195 aluminum alloy could be increasingly strengthened with the more addition of TiB_2, but after a summit more TiB_2 would defer the properties (Xie et al. 2022).

ZL205A aluminum alloy, as a kind of cast aluminum alloy, was wildly used in the industry. Properties of ZL205A are needed to be improved to better adapt to different applications. It is of great importance to fabricate ZL205A/ TiB_2 composites with better performance to tr additional ZL205A alloy. This study aims to investigate the properties of ZL205A/ TiB_2 .

TABLE 1. The Chemical Composition of ZL205A aluminium alloy

Element	Cu	Ti	Mn	Zr	B	Cd	V	Fe	Si	Al
Weight/%	5.07	0.20	0.36	0.08	0.02	0.16	0.14	0.02	0.02	Bal.

TABLE 2. In-situ reaction salt mixture addition

Content of TiB_2(%)	0	0.1	0.5	1.0	2.0	3.0
TiB_2(g)	0	0.5	2.5	5	10	15
K_2TiF_6(g)	0	1.7	7.5	17	34	51
KBF_4(g)	0	1.8	9	18	36	54
Na_3AlF_6(g)	0	0.3	1.5	3	6	9

composites and determine the optimal TiB_2 addition contents to create composites with better performance. ZL205A/TiB_2 Composites with different proportion of TiB_2(0, 0.1, 0.5 , 1.0 , 2.0, 3.0 wt.%) would be produced and compared to study the ZL205A alloy properties under different proportion. In the experiment, TiB_2 are synthesized through in-situ road with addition of the three reaction salts K_2TiF_6, KBF_4, and Na_3AlF_6

MATERIALS AND METHOD

The ZL205A alloy was the basis material for this test, and the specific compositions are listed in the table 1. The samples were categorized into six groups, each group melted 500g of ZL205A aluminium alloy and configured with K_2TiF_6, KBF_4, and Na_3AlF_6 salts in proportion to the TiB_2 content required for each sample as shown in Table 2. The reaction system, with the specific in-situ reaction flow, was as follow formula (1)-(4) (Gao et al. 2016)

$$3K_2TiF_6 + 13Al \rightarrow 3KAlF_4 + K_3AlF_6 + 3Al_3Ti \quad (1)$$
$$2KBF_4 + 3Al \rightarrow 2KAlF_4 + AlB_2 \quad (2)$$
$$AlB_2 + Al_3Ti \rightarrow 4Al + TiB_2 \quad (3)$$
$$3K_2TiF_6 + 6KBF_4 + 10Al \rightarrow 3TiB_2 + 9KAlF_4 + K_3AlF_6 \quad (4)$$

The schematic diagram of the experiment is shown in Figure 1. Firstly, about 500 g of ZL205A alloy matrix in 6 groups were weighed and melted in a resistance furnace. Next, K_2TiF_6, Na_3AlF_6 and KBF_4 powders were weighted according to Table 2. The salt mixture was then milled for 10 minutes to obtain a homogeneous mixture.

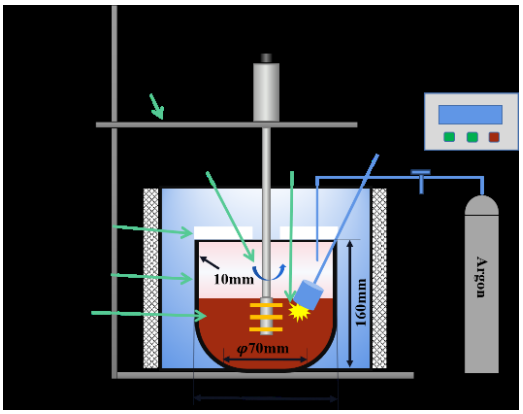

FIGURE 1. Casting schematic diagram

The alloy is placed in a crucible which was heated to 750°C by a resistance furnace . The furnace was set the to 720 °C after the temperature reaches 750 °C. Once the temperature reaches 720 °C, The aluminum foil-wrapped mixture of salts is added to the melt and mechanically stirred for 3 minutes using a graphite impeller at 200 r/min. After the stirring process is completed, remove the scum on the surface of the melt and perform dehydrogenation. Finally, the furnace was turned off, and melt would be left in the furnace until cooling down to ambient temperature.

Before analysis, the samples were ground and polished and will be corroded and then observed using a

metallographic microscope (DSX500, Japan), the linear intercept method (ASTM 112-10) was used to calculate the grain size. In this experiment an electronic universal testing machine was used to tensile the sample at room temperature (25°C) at a tensile rate of 2 mm/min to acquire the YS, EL and TS of the samples. To better investigate the mechanical properties, tensile experiments was repeated five times for each group of samples. Finally the wear resistance experiments are employed to test its wear properties.

RESULTS AND DISCUSSION

Microstructures are shown in Figure 2. In the TiB_2-free ZL205A alloy base material (Figure 2(a)), coarse dendrites can be found with an average grain size as high as 184 μm. The introduction of TiB_2 refine the grain obviously. As shown in Figure 2(b), the addition of 0.1 wt.% of TiB_2 contents resulted in the refinement of the dendrites in the microstructure of ZL205A and the transformation to equiaxed crystals, and the grain size was obviously reduced. When the content of TiB_2 rises to 1.0 -2.0 wt.%, the size of the grains is further refined, and the grains are mainly equiaxed crystals. Nevertheless, when the TiB_2 content reached 3.0 wt.%, the tendency of further grain size refinement was greatly reduced as shown in Figure 3. The grain sizes of the composites were 162 μm, 148 μm. 134 μm, 122 μm and 120 μm. TiB_2 particles act as a core for heterogeneous nucleation and reduce the nucleation free energy (Zhang et al. 2020). However, not all TiB_2 particles become α-Al nucleated, and during solidification, TiB_2- reinforcing particles are accumulated at the solidification front, resulting in a loss of nucleation ability.

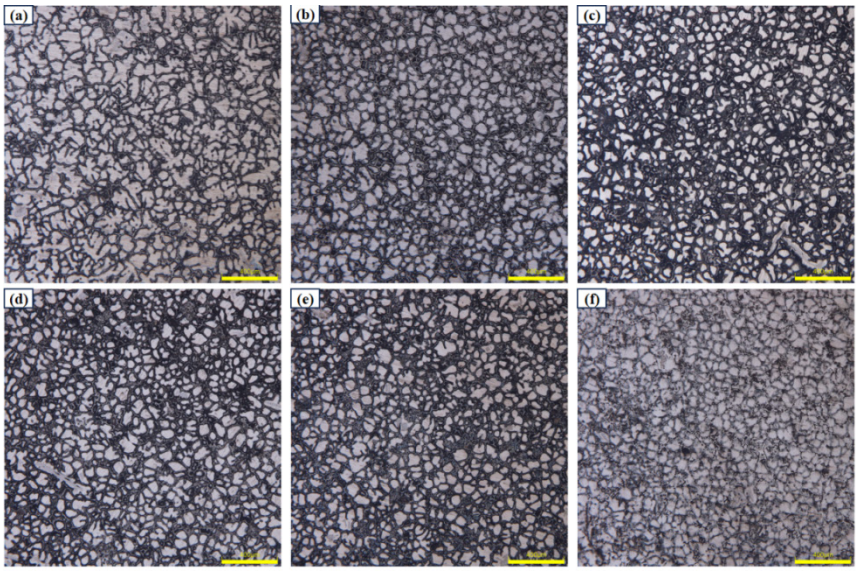

FIGURE 2. Microstructure of ZL205A/TiB_2 composites with different weight proportion of TiB_2 (a)common ZL205A, (b) 0.1wt.% TiB_2, (c) 0.5wt.% TiB_2, (d) 1.0wt.% TiB_2, (e) 2.0wt.% TiB_2, (f) 3.0wt.% TiB_2

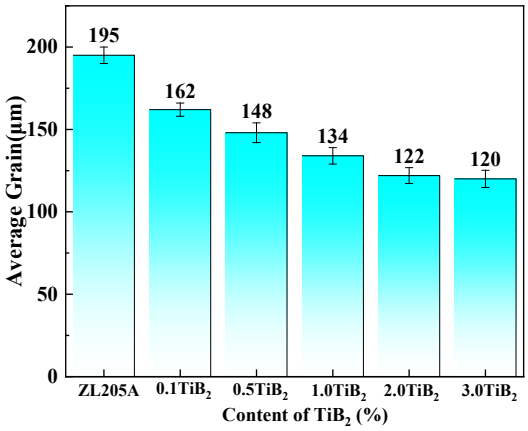

FIGURE 3. Grain size for different groups

As is shown in Figure 4, Ti could be found in the eutectic phases, which prove TiB_2 exists in the eutectic phase with the addition of TiB_2 through In-situ method. The eutectic phase of ZL205A (without addition of TiB_2) generated in agglomeration at the grain boundaries, as is shown in Figure 5a. With the addition of TiB_2 (Figure 5b-f), Eutectic phase are scattered to different level, which is beneficial to the mechanical properties of ZL205A, with the increasing content of TiB_2 content. These are mainly attributed to the grain refinement induced by the addition of TiB_2. Grain refinement provides more boundaries for the space to form fine eutectic phase and inhibit the formation of coarse eutectic phases (Agrawal et al. 2023). But more porosity and Al_3Ti are shown when the content of TiB_2 increase to 3 wt.%, which would deteriorate the mechanical properties of the material. TiB_2 could easily agglomerate during the solidification process with excessive addition of TiB_2. In the solidification process, due to the different coefficients of thermal expansion of TiB_2 particles and Al matrix, voids may remain at the aggregation of TiB_2 particles, and it is possible to form incomplete TiB_2 particles by adding too much salt, which leads to the underutilization of Ti elements, and the coarse Al_3Ti phase could form after that. There exists the optimal content of TiB_2, excessive addition of TiB_2 not only improve the mechanical properties of materials, but effect it negatively.

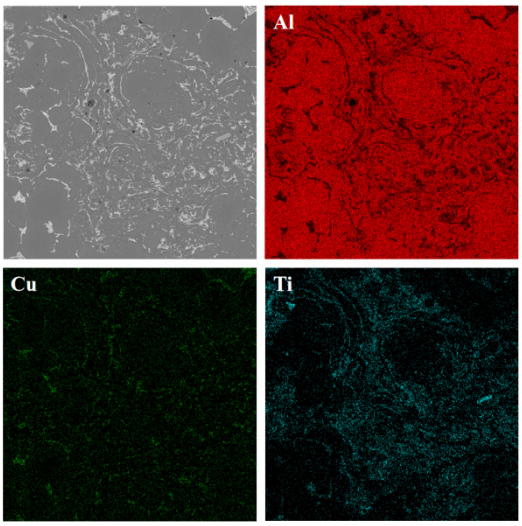

FIGURE 4. EDS energy spectrum pictures of ZL205 with 2 wt.% TiB2

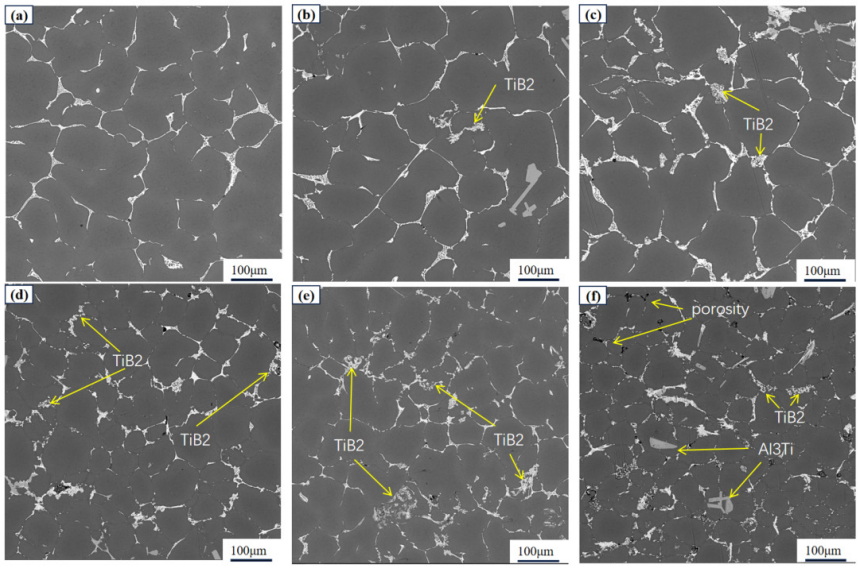

FIGURE 5. Eutectic phase of (a)ZL205A (without TiB_2) (b)with 0.1 wt.% TiB_2, (c)with 0.5 wt.% TiB_2, (d) with 1.0 wt.% TiB_2, (e) with 2.0 wt.% TiB_2, (f) with 3.0 wt.% TiB_2

UTS, YS and EL tests were carried out for samples and the results are shown in Figure 6. The UTS, YS and EL properties of ZL205 composites were effectively enhanced with the addition of TiB_2 content and the strengthening effect was gradually improved with the increase of content. At 2 wt.% TiB_2 content, UTS, YS and EL reach maximum values of 187.5 MPa, 110 MPa and 7%, respectively. When the TiB_2 content is further increased to 3 wt.%, UTS, YS and EL show a decline compared to 2 wt.%.

As is found in the experiment, the mechanical properties of ZL205 cannot be improved continuously with unlimited addition of TiB_2. The addition of 2wt.% TiB_2 is a comparatively optimal addition content for the ZL205/ TiB_2 composites. As is shown in Fig 5, TiB_2 tends to agglomerate with further addition of TiB_2 to 3wt.%. Voids induced by the agglomeration of TiB_2 easily transfer to the source of crack under exterior pressure.

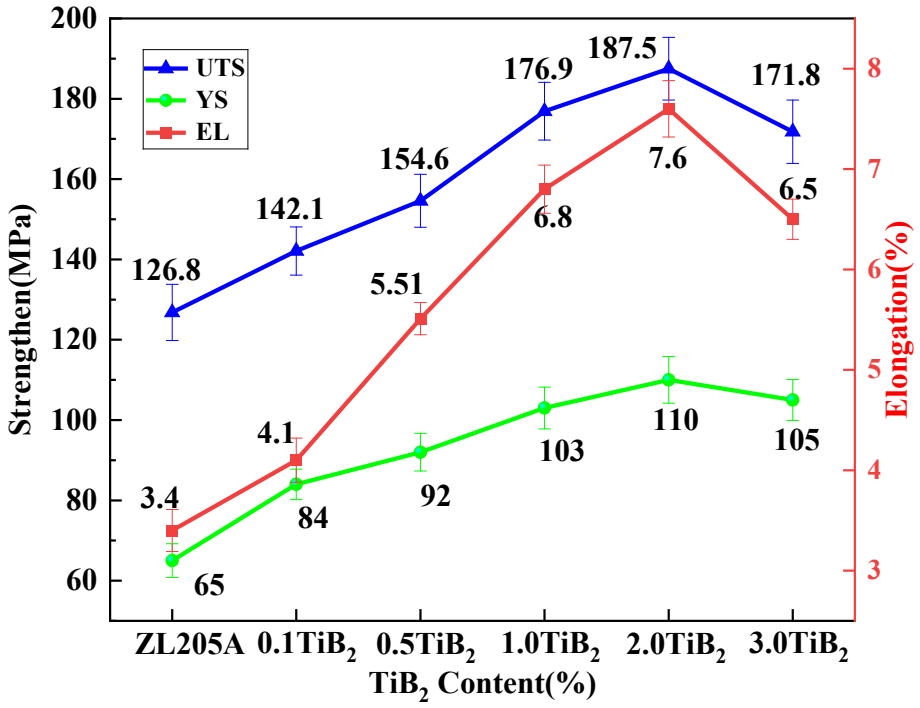

FIGURE 6. average value of TS, YS and EL

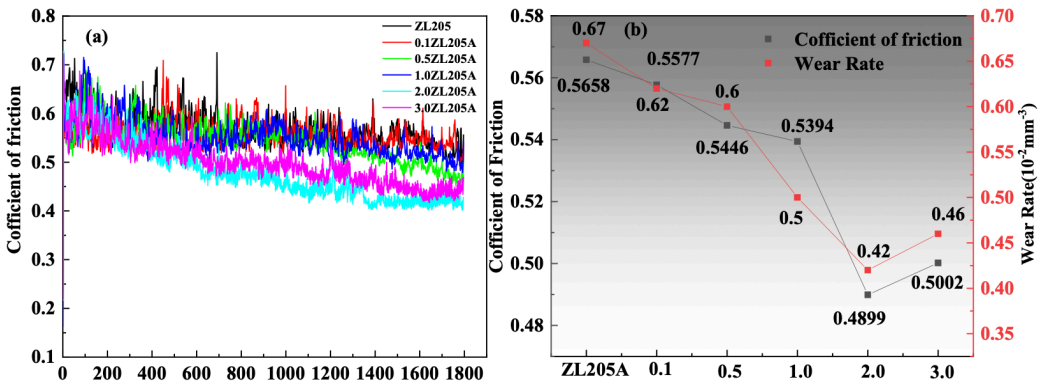

FIGURE 7. (a) coefficient of friction curve of TiB2/ZL205A composites, (b) Wear rate of each group of TiB2/ZL205A composites

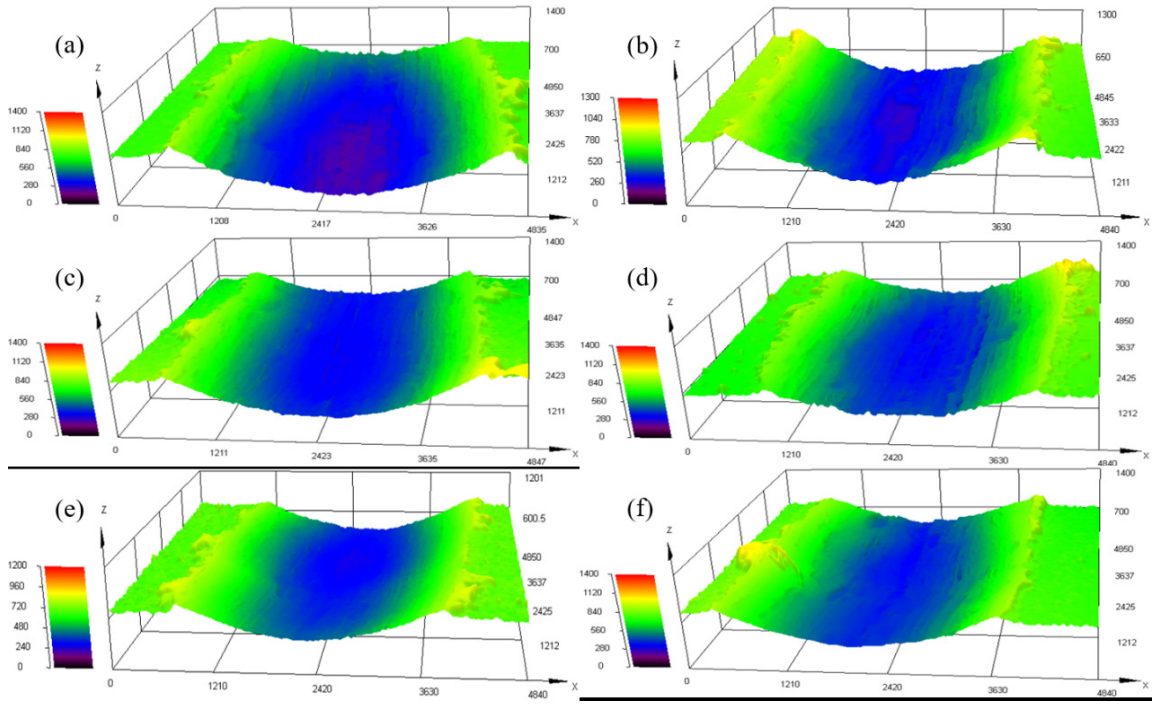

FIGURE 8. 3D morphology of wear test samples(a) ZL205A alloy , (b) Composites with 0.1 wt.% TiB_2 , (c) Composites with 0.5 wt.% TiB_2, (d) Composites with 1 wt.% TiB_2, (e) Composites with 2 wt.% TiB_2, (f) Composites with 3 wt.% TiB_2

Figure 7 demonstrates the wear rate of each group of samples at 30N loads. As shown in 7(b), the wear rate of ZL205A matrix alloy is $0.67 \times 10^{-3}mm^3/Nm$. The wear rate decreases with the introduction of TiB_2, and the wear rate reaches a minimum of $0.42 \times 10^{-3}mm^3/Nm$ when the reinforcing TiB_2 particles are 2.0 wt.%, which is a relative reduction of 37.3%, while the wear rate of 3.0 wt.% TiB_2/ ZL205A composite had a wear of $0.5394 \times 10^{-3}mm^3/Nm$, which exhibit more wear lose happened compared to sample with 2.0 wt. % TiB_2.

Figure 7a shows the friction factor for samples, which constantly varied over the course of the experiments. There are two periods in the friction process, which are the run-in period and steady abrasion period. In the run-in period, the surface of the test specimen wears more and the friction factor fluctuates greatly during the course of the experiment. the friction factor curves of the ZL205A specimens and the friction factor curves underwent large fluctuations during the experiments even at the steady abrasion period. It suggests the inferior abrasion resistance of the material and the long run-in period (Xu et al. 2017). In contrast, the samples of ZL205A composites show better wear resistance. Especially when the content of TiB_2 is raised to 2.0 wt.%, the friction factor curves are obviously stable than the ZL205A and step into stable wear period quickly. However, after raising the TiB_2 content to 3.0%, the fluctuation of the friction factor curve was greater than that at a TiB_2 content of 2.0.

Figure 7b shows the coefficient of friction and wear rate for different samples. As we can see the coefficient of friction fluctuate with the wear rate. Samples with lower coefficient obtained lower wear rate. This phenomenon could be attributed to the shear stresses, which is directly related to the frictional force. A low coefficient of friction leads to lower shear stress, which reduces the likelihood of surface damage such as micro-cracking, plowing, or material transfer (Tien et al. 2021).

According to the experimental results, it can be derived that the TiB_2 addition can reduce the entering time of stable abrasion, reduce the friction coefficient of abrasion, and ultimately improve the wear resistance of ZL205A. However, excessive addition of TiB_2 may negatively affect the friction properties. This could be attributed to the agglomeration of particles when the addition of TiB2 particles increases to 3.0 wt.%, which reduce the strength of bonding between substrate and reinforcements (Zhu et al. 2019). Furthermore, according to Figure 4-12(b), when the TiB_2 particle content is 3.0 wt.%, the traditional mechanical stirring process is unable to fully disperse the particle agglomerations in the aluminum melt, having little impact on enhancing wear resistance. Overall, the uniformly distributed TiB_2 particles can effectively improve the hardness of ZL205A composites, reduce the coefficient of friction of the material, reduce the wear of the material in the process of force, and reduce the area of adhesive wear. Under the action of external forces, the reinforcing

particles TiB_2 are prone to detach from the worn surface, causing defects such as grooves on the matrix surface, thereby accelerating the wear rate of the composite.

Figure 8 shows the 3D laser morphology of the wear surfaces of ZL205A composites with different percents of TiB_2. It mainly presents the three-dimensional structure of the friction wear surface, in which the blue color indicates the lower area and the green color indicates the higher area, and the larger the blue to purple area tends to indicate that the friction wear is more serious. As shown in Figure 8, there is a high percentage of blue areas and even purple areas in (a), indicating that the original ZL205A alloy is more severely worn in the test, which is in line with the results of Figure 7. According to Figs. 8(a)-(f), the proportion of blue area in the graph decreases to different degrees with the increase of TiB_2, and when the TiB2 content reaches 2.0 wt.%, the proportion of blue area in the composite reaches the minimum value, as shown in Figure 8(e), which indicates that it has a relatively good wear-resistant property. When the TiB2 content was further increased to 3%, the blue area increased compared to the 2 % specimen, as shown in Figure (f). The presence of some TiB2 particle agglomerates in 3.0 wt.% ZL205A/ TiB2 composites,as shown in Figure 5(f), could be the reason for the decrease in wear resistance. Defects such as pores are easily formed at the agglomerates, and during frictional wear, the reinforcing particles are easily dislodged from the defects in the matrix, resulting in a lower abrasion performance of the composites.

As shown in Figure 9, the wear width was measured in the SEM images of different composite wear tracks. The wear track widths of the composites samples with TiB_2 content of 0%,0.1%,1% and 2% are 4.2mm, 4.02mm, 3.92mm, 3.81mm, respectively, where the original ZL205A has the largest width of the wear track, and his wear resistance is poorer, which is in line with the conclusions drawn in Figure 8. As shown in Figure 9 (b-d), the abrasion tracks widths were reduced by 4.2%, 6.7%, and 9.3%, respectively.The width of the wear track gradually becomes narrower with the increase of TiB_2 content, indicating that the addition of TiB_2 can effectively improve the wear resistance of TiB_2/ZL205A compliant materials.

The elemental composition characteristics of the friction surface were analyzed through energy dispersive spectroscopy (EDS), with corresponding results presented in Figure 10. As demonstrated in Figure 10(a), the scanning electron microscopy (SEM) morphology reveals the surface topography of the wear specimen. The EDS mapping analysis Figure (b-h) identifies significant oxygen enrichment on the tribological interface, in conjunction with the base alloy constituents (Al, Cu, V) of the composite material. This elemental distribution pattern suggests potential surface oxidation occurring during the wear process.

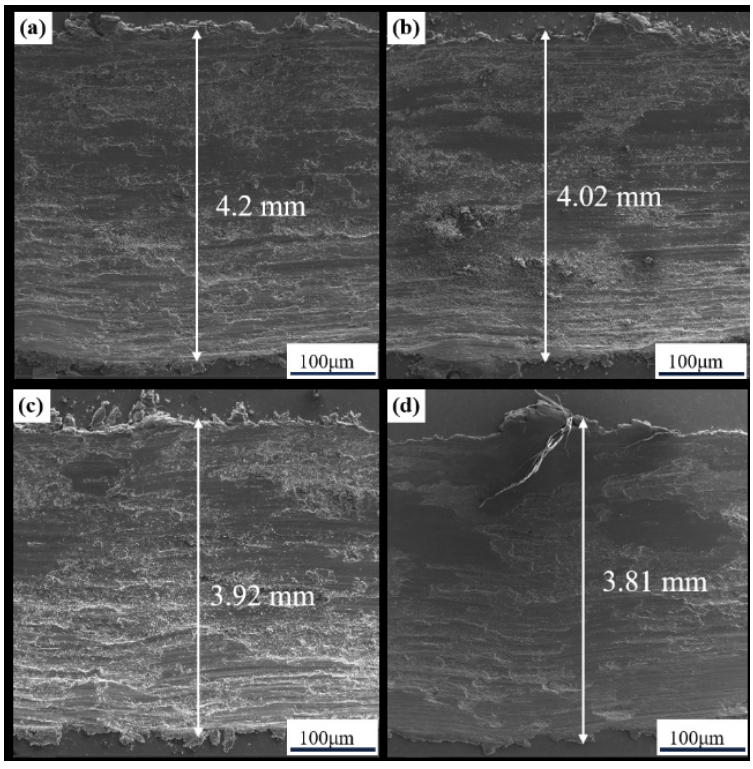

FIGURE 9.Wear track width of : (a) ZL205A , (b) 0.1 wt.% ZL205A/TiB2 Composites, (c) 1.0 wt.% ZL205A/TiB2 Composites, (d) 2.0 wt.% ZL205A/TiB2 Composites

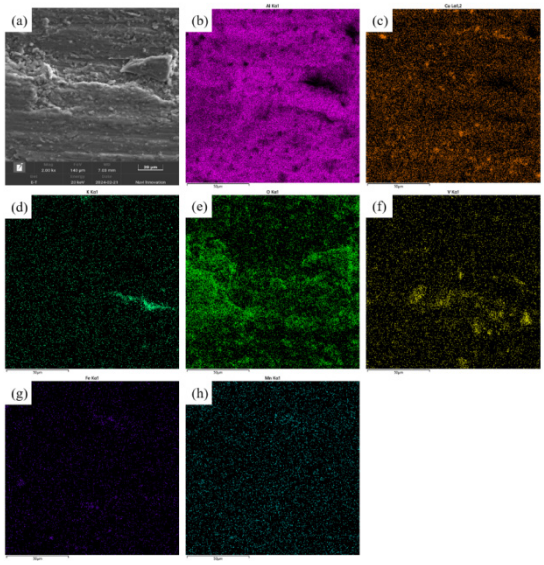

FIGURE 10. EDS Results of the Friction and Wear Surface of ZL205A/TiB2 Composites(a)the SEM of ZL205A/TiB2 , EDS of (b) Al (c) Cu (d) K (e) O(f) V(g) Fe(h)Mn

These observations collectively demonstrate an oxidative wear mechanism characterized by substantial surface oxidation during tribological testing. Metallographic analysis further revealed significant copper deposition on the wear track due to the presence of Al_2Cu intermetallic precipitates. As hard phase constituents within the alloy matrix, these second phase exhibit distinct mechanical behavior under stresses. During wear testing, these coarse Al_2Cu eutectic phases exhibit preferential detachment from the metallic substrate, with subsequent exposure at the wear interface. The accelerated surface degradation arises from two synergistic mechanisms: (1) The pronounced hardness difference between the Al_2Cu precipitates and the aluminum matrix promotes interfacial stress concentration during load-bearing conditions. (2) The weak interfacial cohesion energy between the eutectic phases and matrix facilitates crack nucleation at phase boundaries. This interfacial incompatibility creates localized stress concentrations that ultimately accelerate interfacial decohesion and particulate liberation.

CONCLUSION

The addition of TiB_2 particles during the casting process of ZL205A can effectively refine the microstructure. The coarse dendritic crystals are refined and begin to transform into equiaxed crystals. The degree of grain refinement increases with the increase in TiB_2 content.

The addition of TiB_2 can effectively disperse the eutectic phase, which is conducive to obtaining better mechanical properties of ZL205A, but the addition of too much will lead to the agglomeration of TiB_2. The agglomerated TiB_2 could retain the void during the solidification process, which effect the properties of materials negatively.

Properties, such as tensile strength and wear resistance could be improved effectively with the addition of TiB_2. The strengthening effect also increases with the increase of TiB_2 content.

However, when the TiB_2 content exceeds 2 wt.%, the grain refinement effect of the particles starts to weaken. Composites with 3 wt.% TiB_2 exhibit worse mechanical properties compared to those with 2 wt.% This suggests that there is an optimum value for TiB_2 addition and that excess TiB_2 particles may aggregate and degrade their mechanical properties. In the future, advanced equipment and analysis would be employed to further study the mechanism.

ACKNOWLEDGEMENT

This work was supported by the Education Department of Hunan Province, China (Grant no. 23C0478), and the Universiti Kebangsaan Malaysia (UKM), Malaysia (Grant no. TAP-K007539).

DECLARATION OF COMPETING INTEREST

None.

REFERENCES

Agrawal, A. P., & Srivastava, S. K. 2024. Investigating the effects of adding Si3N4 on microstructural and mechanical characteristics of AA7075-based TiB2-reinforced hybrid MMCs. International Journal of Metalcasting 18(3): 2545-2561.

Aldy, J. E., & Halem, Z. M. 2024. The evolving role of greenhouse gas emission offsets in combating climate change. Review of Environmental Economics and Policy 18(2): 212-233.

Bhowmik, A., Dey, D., & Biswas, A. 2021. Comparative study of microstructure, physical and mechanical characterization of SiC/TiB2 reinforced aluminium matrix composite. Silicon 13(6): 2003-2010.

Chandel, R., Sharma, N., & Bansal, S. A. 2021. A review on recent developments of aluminum-based hybrid composites for automotive applications. Emergent Materials 4(5): 1243-1257.

Dayanand, S., & Babu, B. S. 2020. A Review on synthesis of AlB2 reinforced aluminium matrix composites. In IOP Conference Series: Materials Science and Engineering (Vol. 810, No. 1, p. 012038). IOP Publishing.

Dong, B. X., Li, Q., Wang, Z. F., Liu, T. S., Yang, H. Y., Shu, S. L., ... & Zhang, L. C. 2021. Enhancing strength-ductility synergy and mechanisms of Al-based composites by size-tunable in-situ TiB2 particles with specific spatial distribution. Composites Part B: Engineering 217: 108912.

Fadzil, M., Abdullah, A. B., Samad, Z., Yusof, F., & Manurung, Y. H. P. 2021. Application of lightweight materials toward design for sustainability in automotive component development. In Design for Sustainability (pp. 435-463). Elsevier.

Gao, Q., Wu, S., Lü, S., Xiong, X., Du, R., & An, P. 2017. Effects of ultrasonic vibration treatment on particles distribution of TiB2 particles reinforced aluminum composites. Materials Science and Engineering: A, 680: 437-443.

Graf, A. 2021. Aluminum alloys for lightweight automotive structures. In Materials, design and manufacturing for Lightweight Vehicles (pp. 97-123). Woodhead Publishing.

Kumar, A., Singh, V. P., Singh, R. C., Chaudhary, R., Kumar, D., & Mourad, A. H. I. 2024. A review of aluminum metal matrix composites: fabrication route, reinforcements, microstructural, mechanical, and corrosion properties. Journal of Materials Science 59(7): 2644-2711.

Malaki, M., Xu, W., Kasar, A. K., Menezes, P. L., Dieringa, H., Varma, R. S., & Gupta, M. 2019. Advanced metal matrix nanocomposites. Metals 9(3): 330.

Srivyas, P. D., & Charoo, M. S. 2019. Application of hybrid aluminum matrix composite in automotive industry. Materials Today: Proceedings 18: 3189-3200.

Srivyas, P. D., & Charoo, M. S. 2019. Application of hybrid aluminum matrix composite in automotive industry. Materials Today: Proceedings 18: 3189-3200.

Tien, C. L. , & Lin, T. W. . 2021. Out-of-plane thermal expansion coefficient and biaxial young's modulus of sputtered into thin films. Coatings 11(2): 153.

Xie, Z., Jiang, R., Li, X., Zhang, L., Li, A., & He, Z. 2022. Microstructural evolution and mechanical properties of TiB2/2195 composites fabricated by ultrasonic-assisted in-situ casting. Ultrasonics Sonochemistry 90: 106203.

Xu, R., Fan, G., Tan, Z., Ji, G., Chen, C., Beausir, B., ... & Zhang, D. 2018. Back stress in strain hardening of carbon nanotube/aluminum composites. Materials Research Letters 6(2): 113-120.

Zhang, Y., Li, R., Chen, P., Yang, Y., Li, X., & Jiang, R. 2020. Tuning the microstructure morphology and genetic mechanical properties of 2219 Al alloy with ultrasonic treatment. Journal of Alloys and Compounds 846: 156251.

Zhu, K., Li, Z., Fan, G., Xu, R., & Jiang, C. 2019. Thermal relaxation of residual stress in shot-peened CNT/Al–Mg–Si alloy composites. Journal of Materials Research and Technology 8(2): 2201-2208.